Supplementary Information Appendix

Super-Swelled Lyotropic Single-Crystals

Hojun Kim, Ziyuan Song, and Cecilia Leal*

Materials Science and Engineering Department and Frederick Seitz Materials Research Laboratory, University of Illinois at Urbana-Champaign, 1304 West Green Street, Urbana, Illinois 61801, United States.

*Corresponding Author: Cecilia Leal (cecilial@illinois.edu)

Chemical structure of lipids used in the study:

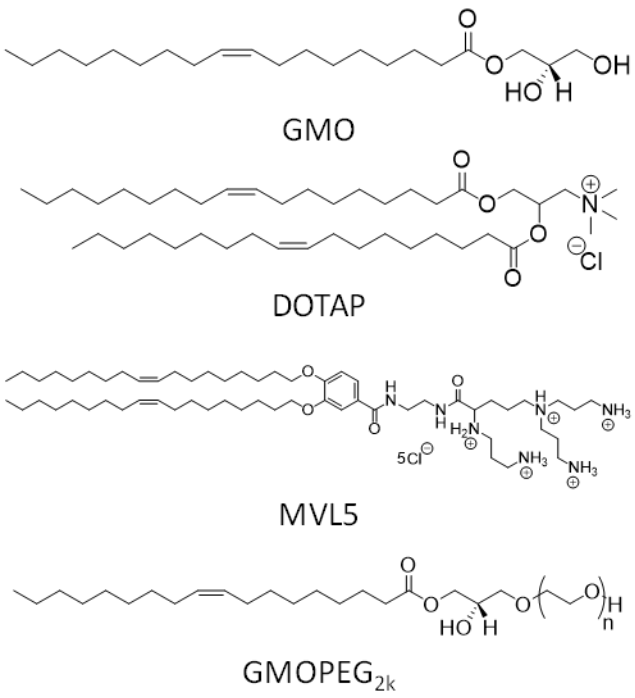

Fig. S1. 1.Glycerol Monooleate (GMO), 2. Net positively charged lipid: 1,2-dioleoyl-3-trimethylammonium propane (DOTAP), 3. Pentavalent lipid: N1-[2-((1S)-1-[(3-aminopropyl)amino]-4-[di(3-amino-propyl)amino]butylcarboxamido)ethyl]-3,4-di[oleyloxy]-benzamide (MVL5), and 4. custom-designed GMO lipid conjugated to 2 kDa polyethylene glycol (GMOPEG).

^{1}H NMR spectrum of a GMO lipid cake where chloroform was dried for 48 hours. (500 MHz, in CD_2Cl_2):

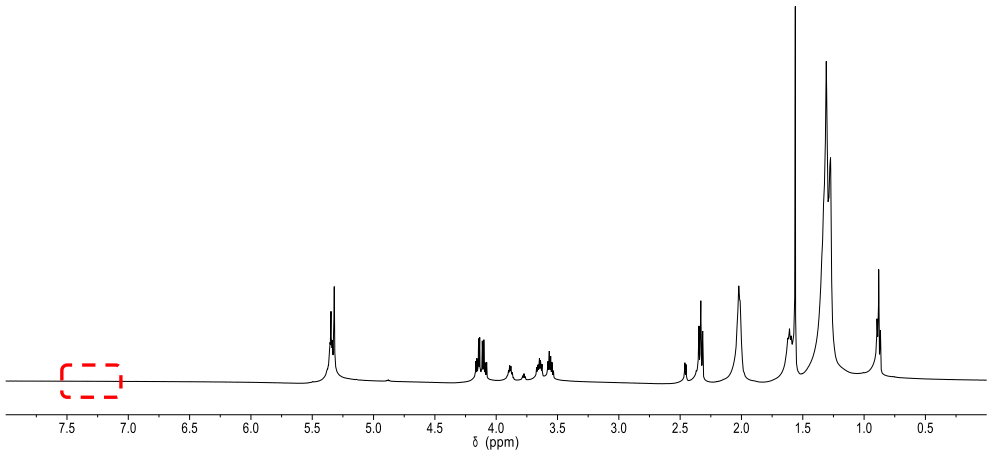

Fig. S2. ^{1}H NMR (CD_2Cl_2): To determine whether there is leftover chloroform residues after drying, the dried lipid cake was dissolved in anhydrous CD_2Cl_2. From the ^{1}H NMR spectrum, no obvious peak was observed around 7.32 ppm, indicating complete removal of chloroform.

SAXS structural study of dried lipid cakes:

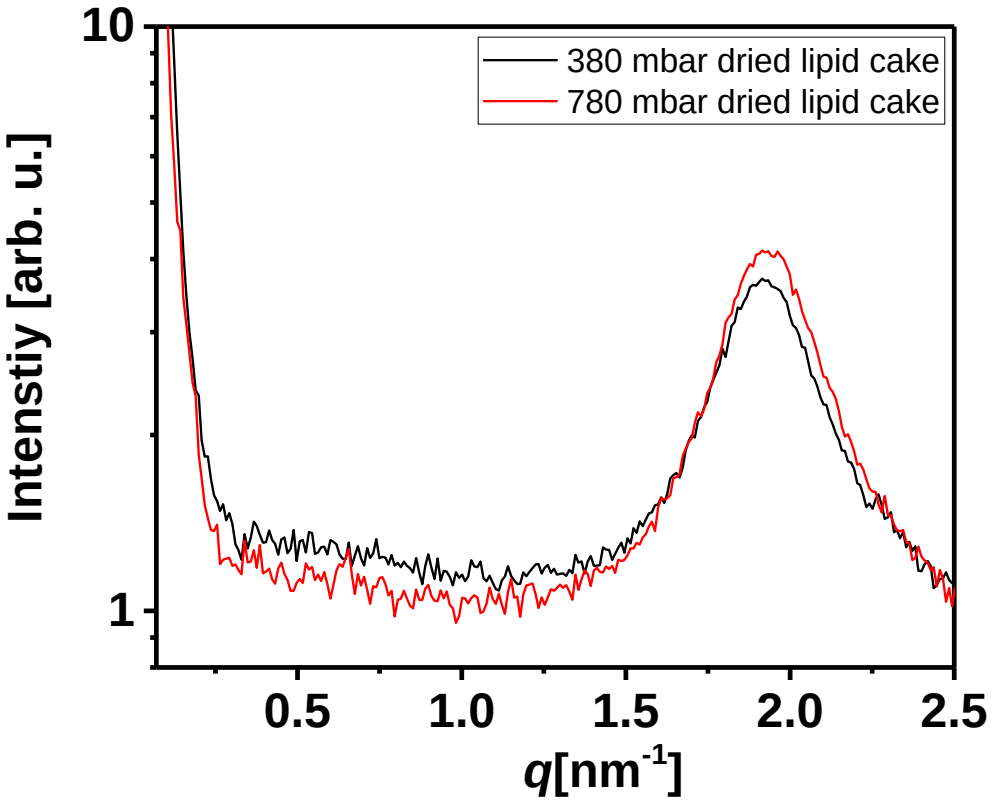

Fig. S3. SAXS scans of dried lipid cakes (GMO/DOTAP/GMOPEG 95/4/1 mole ratio). 1D integrated SAXS scans of fastly dried lipid cake (380 mbar, black line) and slowly dried lipid cake (780 mbar, red line). No structural differences can be detected. One single broad peak corresponding to real spacing of 3.3 nm is observed for both cases.

^{1}H NMR spectrum of GMO in $CDCl_3$ (500 MHz):

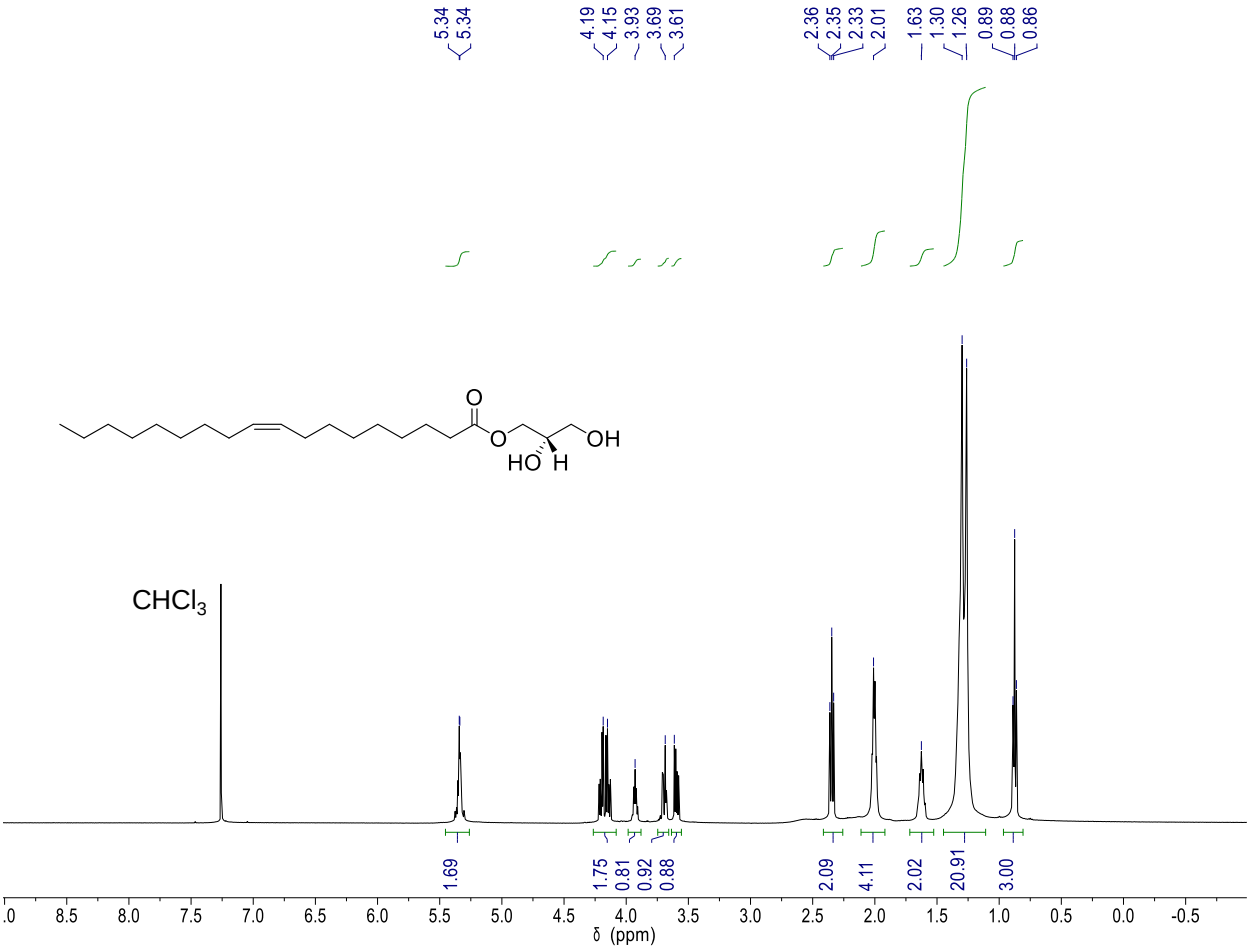

Fig. S4. ^{1}H NMR ($CDCl_3$): δ 5.34 (m, 2H, –CH_2CH=$CHCH_2$–), 4.17 (m, 2H, –$COOCH_2CH(OH)CH_2OH$), 3.93 (m, 1H, –$COOCH_2CH(OH)CH_2OH$), 3.65 (m, 2H, –$COOCH_2CH(OH)CH_2OH$), 2.35 (t, 2H, *J* = 7.6 Hz, –CH_2CH_2COO–), 2.01 (m, 4H, –CH_2CH=$CHCH_2$–), 1.63 (m, 2H, –CH_2CH_2COO–), 1.28 (m, 20H, $CH_3(CH_2)_6$– and –$(CH_2)_4CH_2CH_2COO$–), 0.88 (t, 3H, *J* = 6.8 Hz, $CH_3(CH_2)_6$–).

^{1}H NMR spectrum of DOTAP in $CDCl_3$ (500 MHz):

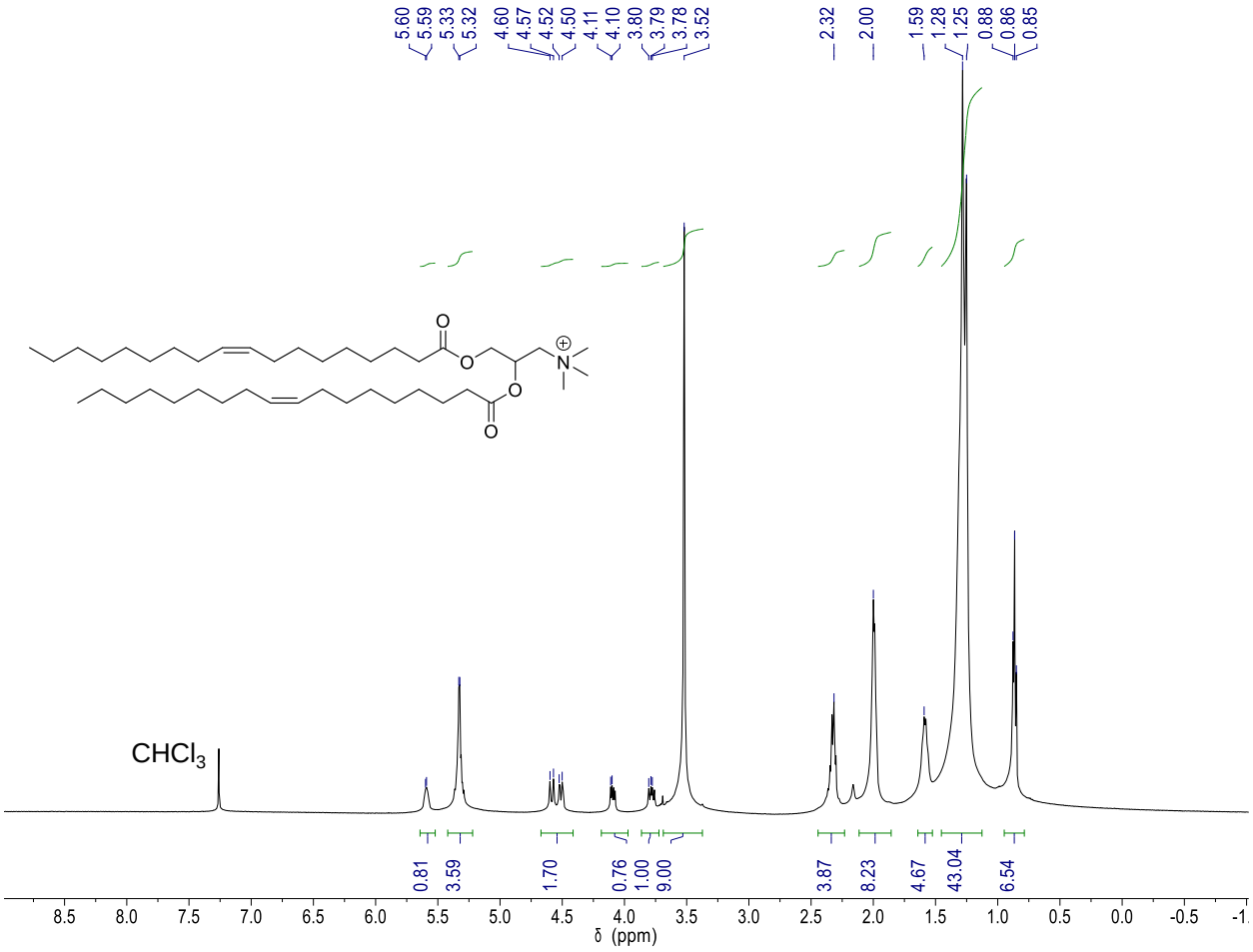

Fig. S5. ^{1}H NMR ($CDCl_3$): δ 5.60 (m, 1H, –COOCH_2C*H*=), 5.32 (m, 4H, –CH_2C*H*=C*H*CH_2–), 4.54 (m, 2H, –COOCH_2CH–), 4.10 and 3.79 (m, 2H, –C$H_2$$N^+$($CH_3$)$_3$), 3.52 (s, 9H, –$CH_2$$N^+$(C$H_3$)$_3$), 2.32 (m, 4H, –$CH_2CH_2$COO–), 2.00 (m, 8H, –C$H_2$CH=CHC$H_2$–), 1.59 (m, 4H, –C$H_2$$CH_2$COO–), 1.26 (m, 40H, CH_3(CH_2)$_6$– and –(CH_2)$_4$$CH_2$$CH_2$COO–), 0.86 (t, 3H, *J* = 6.7 Hz, CH_3(CH_2)$_6$–).

^{1}H NMR spectrum of GMOPEG in $CDCl_3$ (500 MHz):

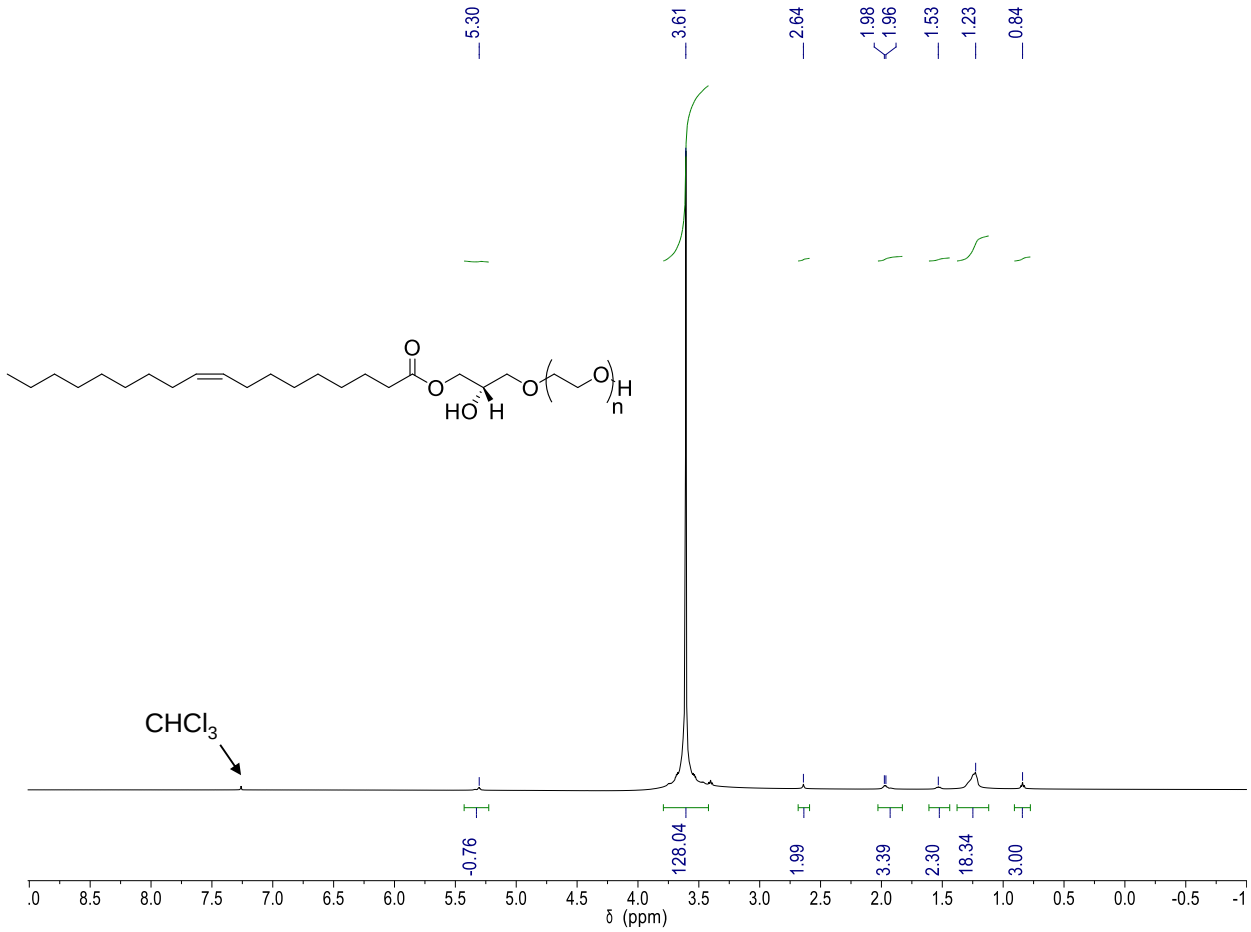

Fig. S6. ^{1}H NMR ($CDCl_3$): δ 5.34 (m, 2H, –CH_2CH=$CHCH_2$–), 3.61 (m, 128H, –$CH2CH_2O$– from PEG units), 2.64 (m, 2H, –CH_2CH_2COO–), 1.97 (m, 4H, –CH_2CH=$CHCH_2$–), 1.53 (m, 2H, –CH_2CH_2COO–), 1.23 (m, 20H, $CH_3(CH_2)_6$– and –$(CH_2)_4CH_2CH_2COO$–), 0.84 (m, 3H, $CH_3(CH_2)_6$–).

Note: some peaks from the oleyl group are invisible since they overlap with the protons on PEG methylene groups.

MALDI-TOF MS spectrum of GMOPEG:

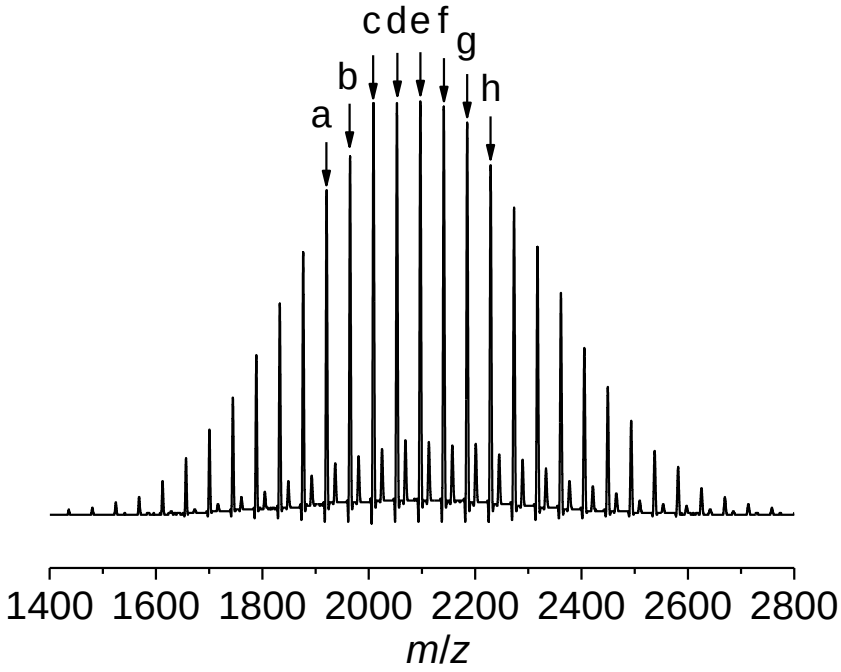

	m/z	n
a	1920.70	35
b	1964.82	36
c	2008.79	37
d	2052.90	38
e	2096.92	39
f	2141.05	40
g	2185.04	41
h	2229.08	42

Fig. S7. The obtained *m/z* shown in the table on the right agrees very well with the calculated value ($[GMOPEG + Na]^+$, $379.28+44.05 \times n$, where n represents the degree of polymerization of PEG).

^{1}H NMR spectrum of fresh, 3 months, and 5 months old large cubic samples in $CDCl_3$ (500 MHz):

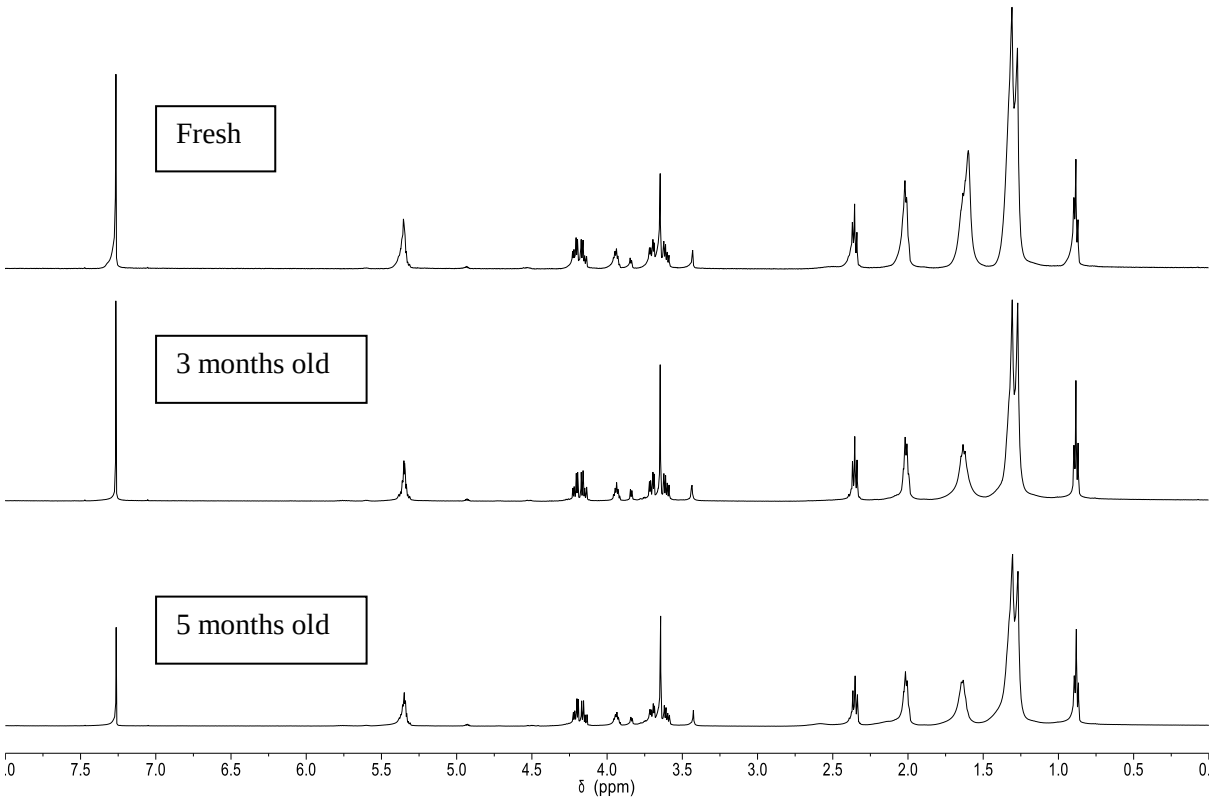

Fig. S8. ^{1}H NMR ($CDCl_3$): Samples freshly prepared as well as 3 months and 5 months old were freeze-dried for 2 hours, and dissolved in $CDCl_3$ for NMR characterization. From the ^{1}H NMR spectra, no obvious change of chemical shift was observed, indicating negligible degradation of lipids (e.g., oxidation of double bonds, hydrolysis of ester bonds) even after 5-months storage.

Incorporation of large citric acid capped (hydrophilic) nanoparticles:

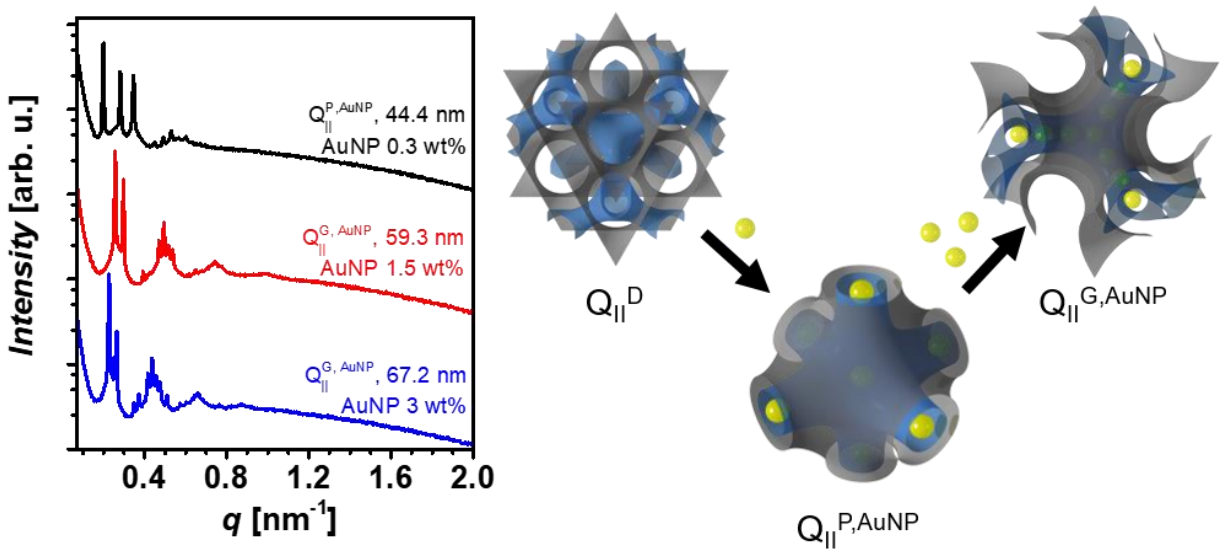

Fig. S9. Demonstration of large solute encapsulation in super-swelled bicontinuous cubic phases. 1D integrated *I* vs *q* data of GMO/DOTAP/GMOPEG (97.5/1.5/1) with three different gold nanoparticle concentrations (0.3, 1.5, and 3 wt% for black, red, and blue lines respectively). At 0.3 wt% gold nanoparticle concentration, a diamond to primitive phase change with 4.4 nm increase in lattice parameter (a^{AuNP} = 44.4 nm) is observed. This is a clear indication of successful incorporation of nanoparticles within the lipid matrix. Increased gold nanoparticle concentration (1.5 wt%) induces another phase change to a gyroid. Further increase of gold nanoparticle concentration (3 wt%) expands the unit cell dimension to 67.2 nm. The illustration depicts the Q_{II}^{D} → $Q_{II}^{P,AuNP}$ → $Q_{II}^{G,AuNP}$ phase transition as a function of increasing amounts of gold nanoparticles (yellow sphere) within the aqueous channels (represented in blue) of the lipid bicontinuous cubic phases (mid-plane of membrane represented as a gray surface). It is noteworthy that a similar phase evolution trend was observed previously with increasing contents of lipids with augmented inter-headgroup repulsions (charged or polymer conjugated lipids, Kim and Leal (2015) *ACS Nano* 9:10214–10226). This encapsulation experiment clearly demonstrates that super-swelled bicontinuous cubic phases are suitable for applications where large drug molecules or proteins are required to be embedded within the bicontinuous cubic network such as drug delivery and protein crystallization.

Bicontinuous lipid cubic single-crystal scattering:

(a)

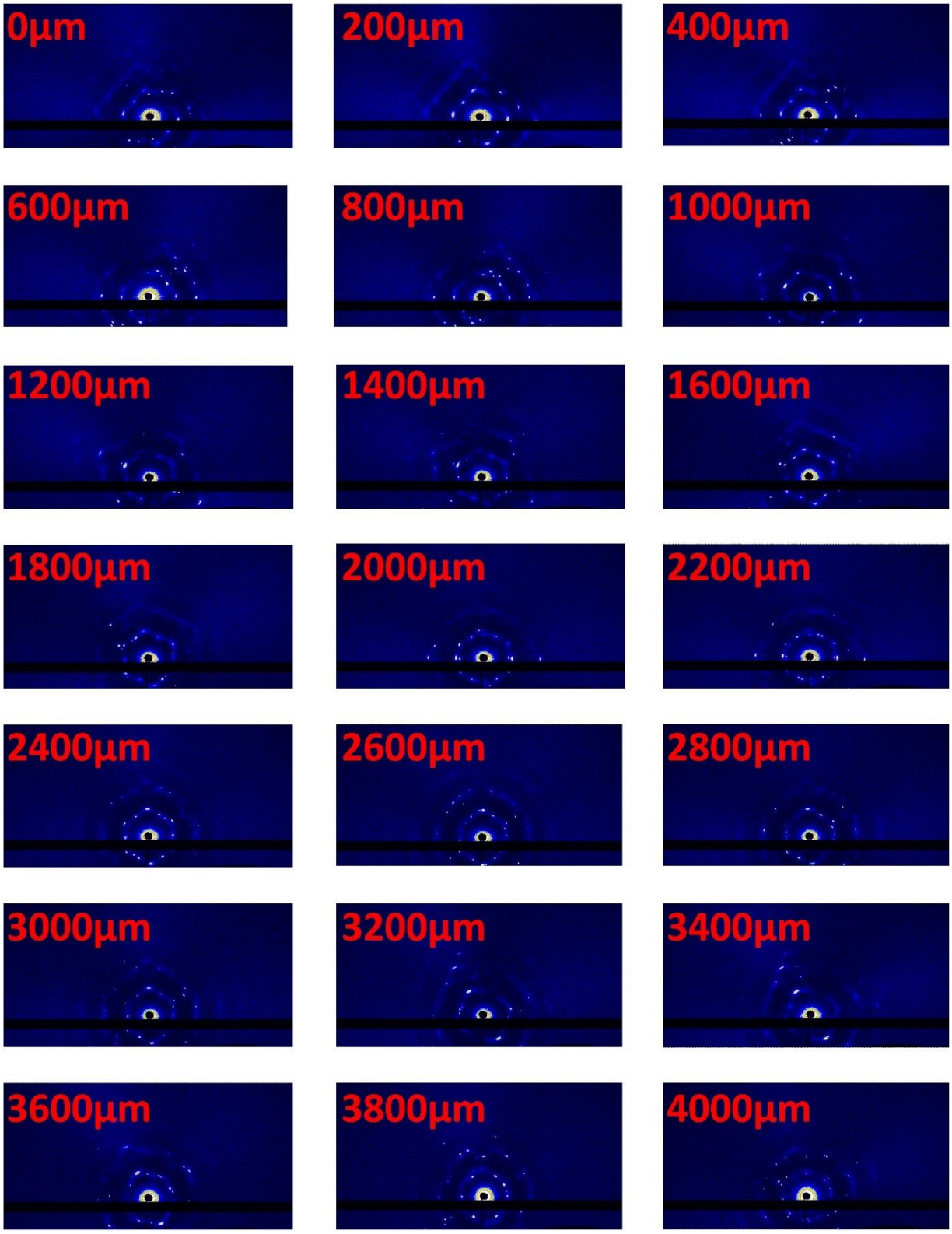

(b)

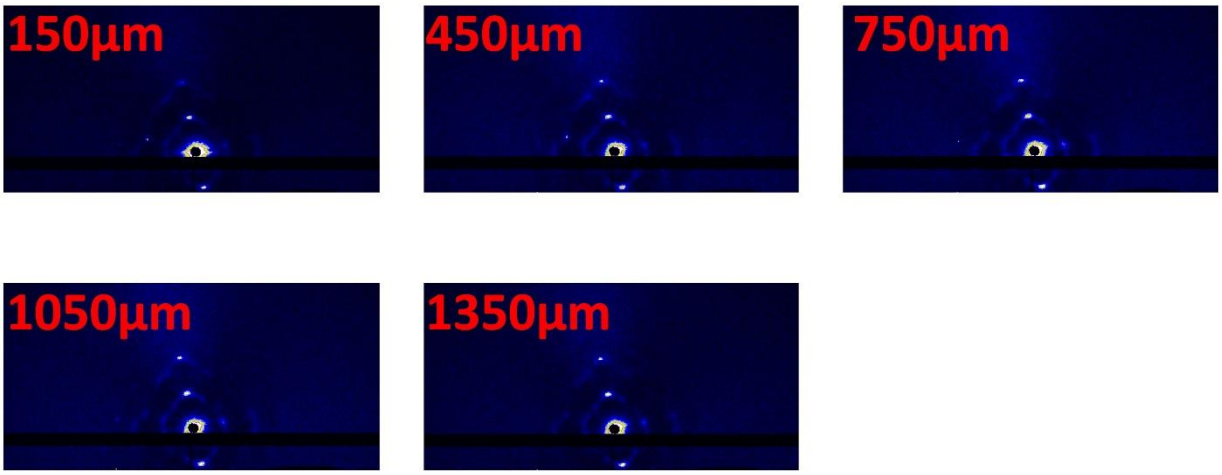

(c)

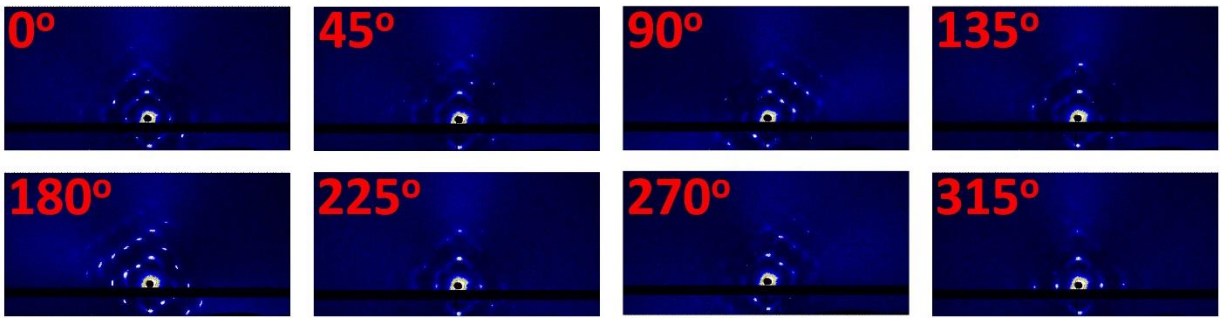

Fig. S10. Small Angle X-ray Scattering (SAXS) scans of GMO/DOTAP/GMOPEG (97.5/1.5/1) at different spatial locations showing single crystal diffraction patterns. (a) Vertical (200 µm step) and (b) horizontal (300 µm step) SAXS scans. (c) Rotational 2D SAXS diffraction patterns of the bicontinuous diamond cubic phase at 45 degree steps. (-1 -1 1) and (1 1 -1) planes are observed at vertical directions regardless of rotations indicating that the rotation axis is parallel to [1 1 -1]. The beam size was about 300 µm x 20 µm (*H* x *V*). Spatial SAXS scans reveal that the single-crystal dimension is ~1 mm^3.

Ewald sphere construction for single-crystal studies:

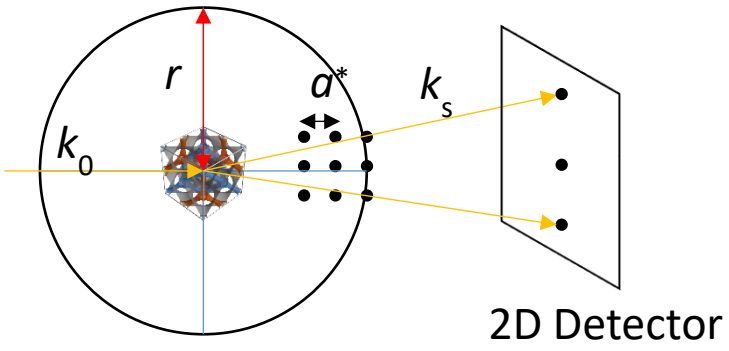

The radius of the Ewald sphere is $r = \lambda^{-1}$ where λ is the wavelength of the X-ray radiation.

For a 14keV X-ray source, E^{photon} = 14keV. Accordingly, $\lambda = hc/E$ = 0.8856Å and r = 1.13 Å^{-1}

$a^* = 2\pi/a = 2\times3.14/414[Å] = 0.0152$ Å^{-1}

As $r >> a^*$, the Ewald sphere is effectively a flat plane up to $6a^*$ in reciprocal space as shown below.

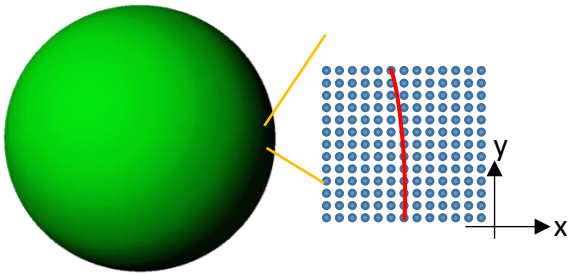

This allows us to find the direction of incoming photons, k_0, by plotting the scattering planes in the reciprocal space. For example, let us consider the following scattering image to find k_0:

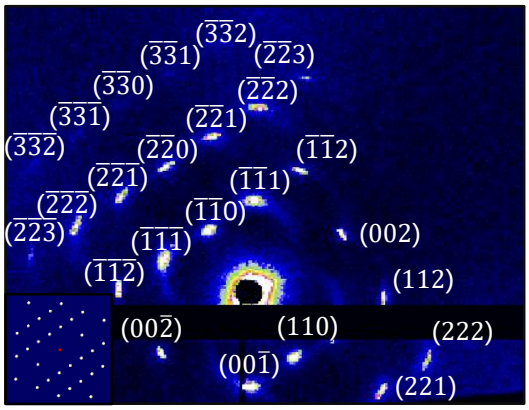

We can assign the plane family of each Bragg peak from the integrated I vs q graph. By simulating the diffraction points at different orientations of the single-crystal, we can index the Bragg peaks more accurately.

With the indexed diffraction patterns, one can plot the scattered planes in the reciprocal space.

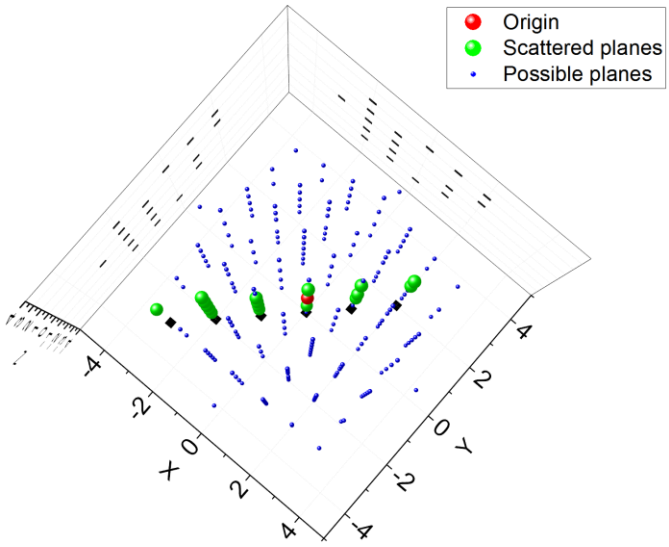

By selecting two random vectors from the surface of the green dots, say $\boldsymbol{u}$ and $\boldsymbol{v}$, the normal vector of the surface can be obtained by the cross product ($\boldsymbol{u} \times \boldsymbol{v}$). In this case, this is parallel to the [1 -1 0] direction. As the Ewald sphere is large enough, this normal vector to the plane is approximately the direction of the incoming beam, k_0.

As the incoming beam direction is known, the rotational axis of the capillary can be obtained by considering incoming beam directions for two different data points. For example,

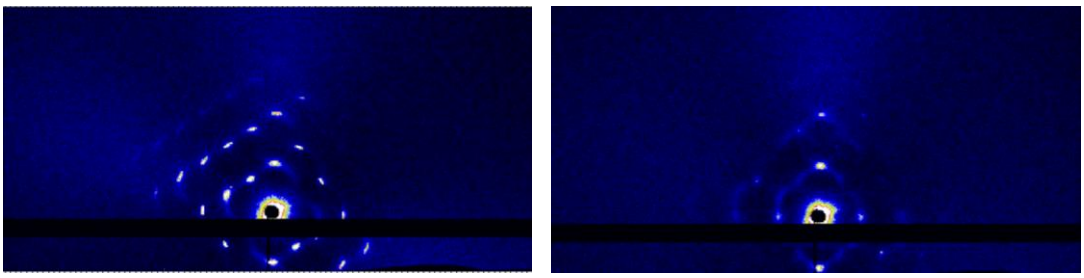

These two images are obtained by rotating 45 degrees along the long axis of the capillary. The incoming beam directions are [1 -1 0] and [1 1 2]. Based on the geometry of our experimental setup shown below, the cross product of these two vectors is the rotational axis which is [-2 -2 2] parallel to [-1 -1 1].

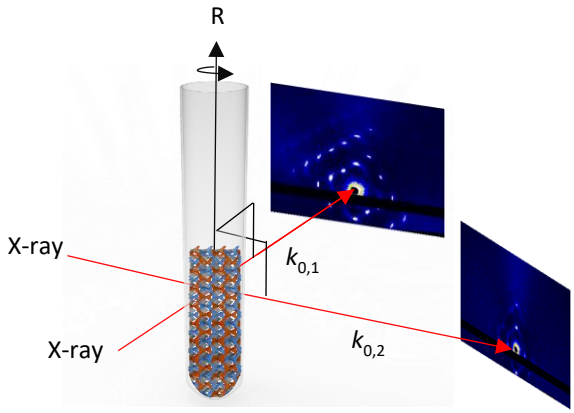

This construction can be also confirmed through a 3D Ewald sphere construction. For example, consider the image below:

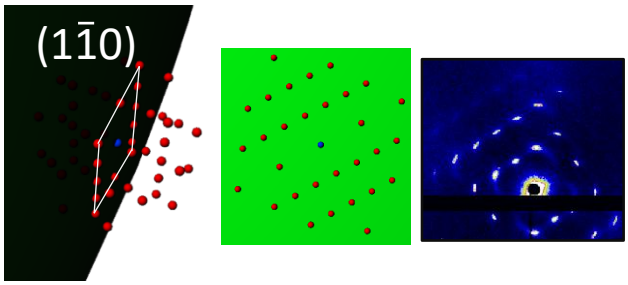

The fact that (-1 -1 1) and (1 1 -1) planes are observed at every rotation angle indicates that the rotation axis is [-1 -1 1]. Importantly, the full construction shown above confirmed that the sample is indeed a single-crystal.

Initial SAXS diffraction pattern of super-swelled bicontinuous diamond cubic phase:

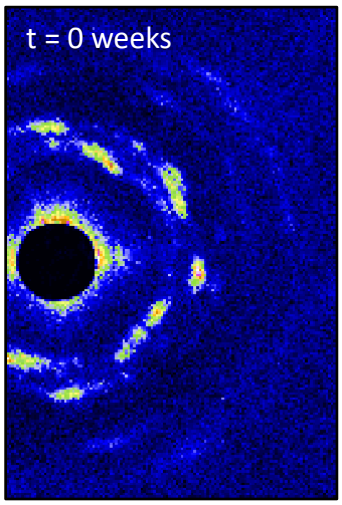

Fig. S11. The 2D SAXS scan image shows a partially aligned polycrystalline structure for the GMO/DOTAP/GMOPEG (97.5/1.5/1) system.

Cryo-EM image of bulk bicontinuous cubic phases:

(a)

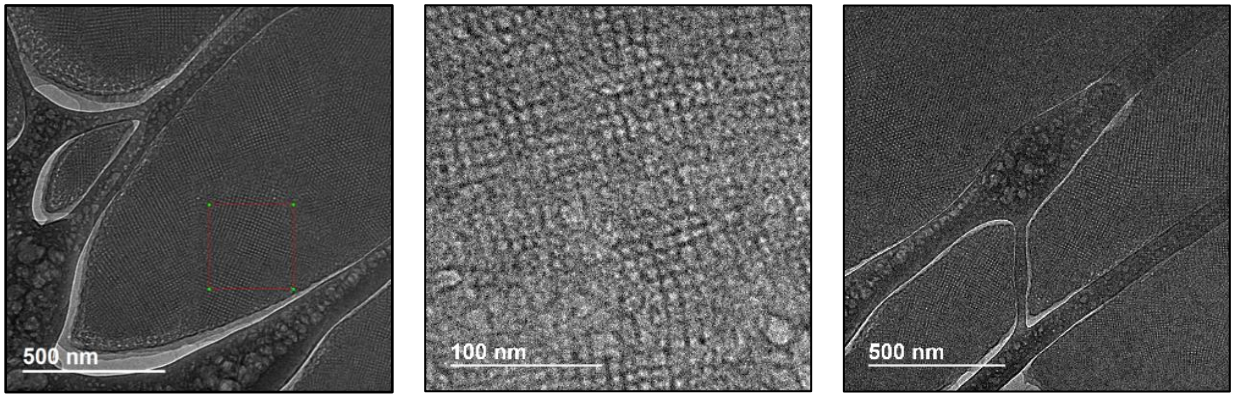

(b)

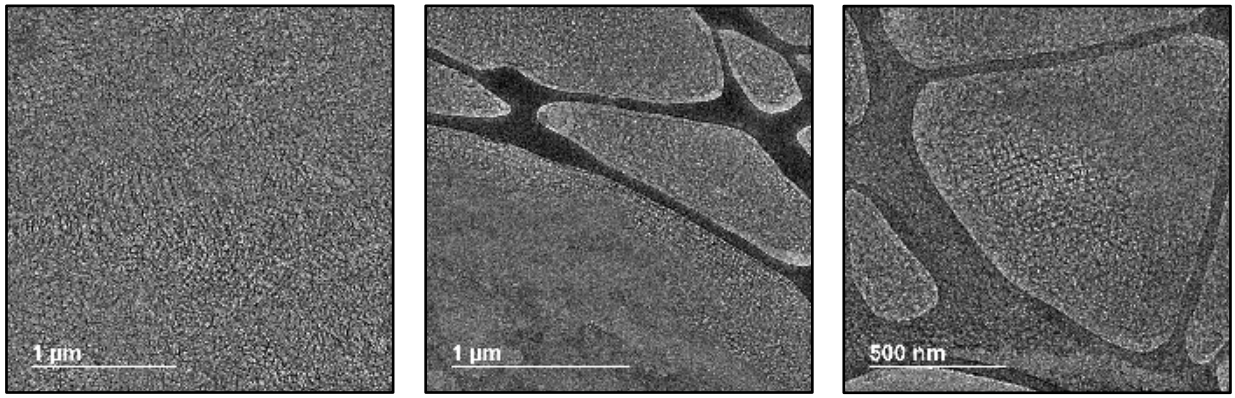

(c)

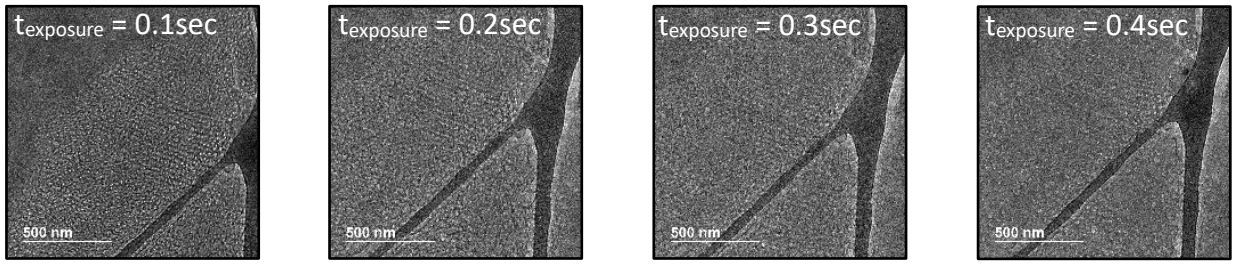

Fig. S12. (a) Regular spacing bicontinuous diamond cubic phase aligned in the (100) and the (111) plane displaying atomic solid like ordering (b) Super-swelled bicontinuous diamond cubic phase aligned in the (110) and the (100) planes. (c) beam damage of super-swelled bicontinuous cubics at 0.1 sec exposure time steps.

^{1}H NMR spectrum of chloroform used in the study in CD_2Cl_2 (500 MHz):

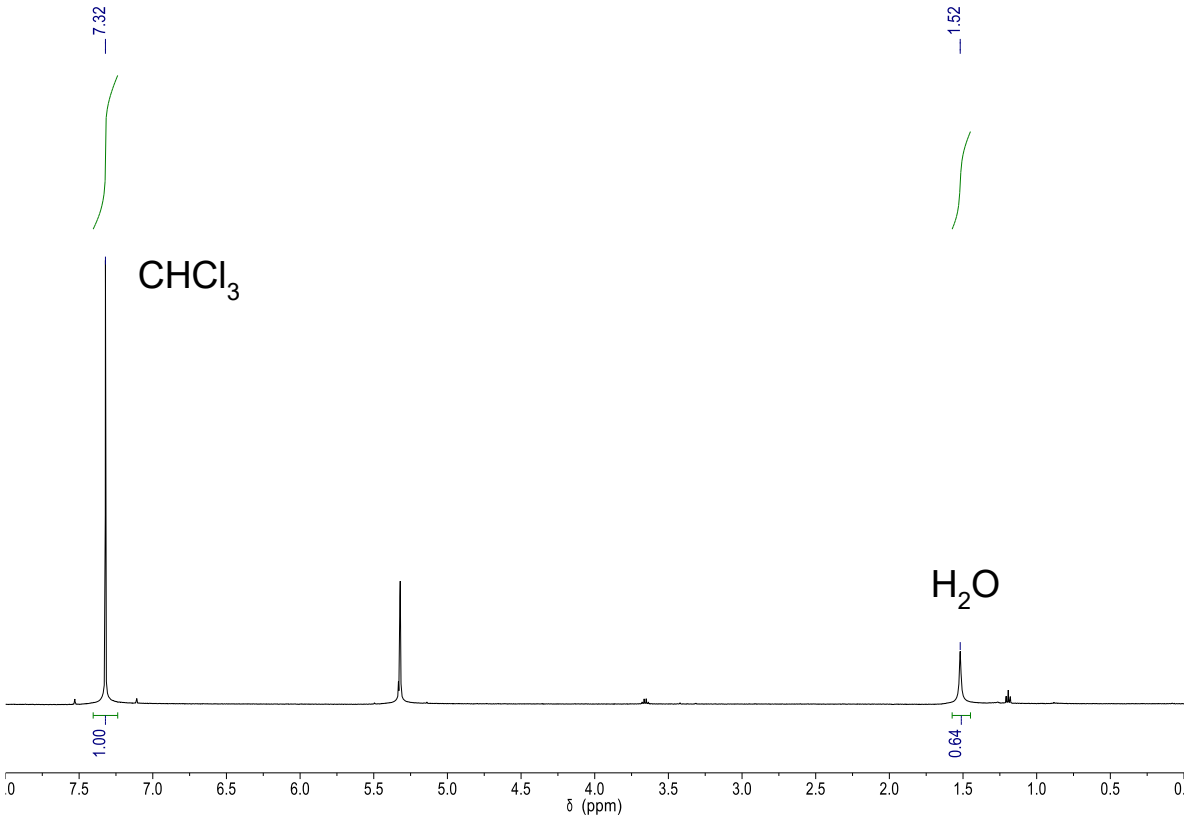

Fig. S13. ^{1}H NMR (CD_2Cl_2): In order to quantify the amount of water in chloroform, chloroform was dissolved in anhydrous CD_2Cl_2. The water content was calculated by comparing the integration of chloroform (7.32 ppm) and water (1.52 ppm), which is determined to be 4.6 wt%. This indicates regular chloroform is good enough to produce the same results.

Materials: We used >99.8% pure chloroform (Sigma Aldrich, MO, USA) as received. Glycerol monooleate (GMO) was purchased from Sigma Aldrich (MO, USA) and PEGylated GMO was custom designed and ordered from NOF America (NY, USA). All other lipids including 1,2-dioleoyl-3-trimethylammonium propane (DOTAP) and N1-[2-((1S)-1-[(3-aminopropyl)amino]-4-[di(3-amino-propyl)amino]butylcarboxamido)ethyl]-3,4-di[oleyloxy]-benzamide (MVL5) were purchased from Avanti polar lipids (AL, USA). All lipids are dissolved in fresh chloroform solvent (Sigma Aldrich, MO, USA) at the desired molar ratios and concentration (GMO: 50 mg/ml, DOTAP and GMOPEG: 25 mg/ml, and MVL5: 10 mg/ml). Citric acid capped 10 nm gold nanoparticle was purchased from Sigma Aldrich (MO, USA).

Non-equilibrium assembly method:

1. Formation of dry lipid cakes: The key feature of non-equilibrium assembly is fast organic solvent evaporation out of lipid mixtures prepared directly in a quartz capillary. First, the desired amount of each lipid in chloroform is transferred into 1.5 mm quartz capillaries (Hilgenberg, Germany). To ensure there is no residual lipids in the wall, quartz capillaries are then centrifuged at 3908.5 G and 25^{o}C (Sorvall ST 16R, Thermo Fisher Scientific, MA, USA) for 2 minutes. The centrifuged solution in the capillary is about 5 mm in length. The capillary is then placed inside of a rotary evaporator (RV 10, IKA, NC, USA) at desired pressure and temperature. For this study, we fixed the temperature at 25^{o}C and varied pressure inside from 380 to 780 mbar. An oil free pump (MaximaDry, Thermo Fisher Scientific, MA, USA) is used to regulate the inside pressure of the rotary evaporator. The chloroform dries out while the sample is rotating inside of the rotary evaporator and drying takes approximately 24, 17, and 12 hours for 780, 580, and 380 mbar, respectively. This drying time was calculated by monitoring the point at which there is no mass change (0.01 mg step scale) and no visible volume change. In order to ensure full removal of chloroform from the dried lipid cakes, all samples are further dried for more than two days. During the drying process, the solution doesn't leave any visible track on the wall. When properly dried, lipid cakes are half-transparent and located at the very bottom of the capillary. There are no visible lipid residues in the walls after drying (please refer to the bottom picture).

2. Lipid-cake hydration: Fully dried samples are hydrated by adding Milli-Q water (Millipore, MA, USA) to make a solution of 0.1 M final concentration (3.86 w/w% of lipid/water for 95/4/1 mole ratio of GMO/DOTAP/GMOPEG). The samples are then centrifuged at 3908.5 G for more than 10 minutes (Sorvall ST 16R, Thermo Fisher Scientific, MA, USA) to ensure efficient water penetration through dried lipid cakes. To prevent water evaporation that changes the lipid concentration, we flame-seal capillaries. The total length of flame-sealed capillaries is about 6 cm.

Finally, the samples are stored at 45 ^{o}C for at least two days before inspection. The inspection of the structures is conduced after the samples equilibrate at room temperature for a couple of hours. Properly prepared samples are always transparent at all points after incubation.

Small Angle X-ray Scattering: Hydrated samples were scanned using a home built (with the help of Forvis Technologies, CA, USA) small angle X-ray scattering machine composed of a Xenocs Genix3D Cu-Ka X-ray source (1.54 Å/8 keV), with ultra-low divergence of ~1.3 mrad. 2D diffraction data were radially averaged upon acquisition on a Pilatus 300 K 20 Hz hybrid pixel detector (Dectris, Switzerland) and integrated using FIT2D software (http://www.esrf.eu/computing/scientific/FIT2D) from ESRF. For MVL5 samples and single-crystal scattering data, we performed transmission SAXS scans at beamline 12-ID-B, Advanced Photon Source at Argonne National Lab. The synchrotron source has an average photon energy of 14 keV with beam size of 300 μm x 20 μm (*H* x *V*).

Cryogenic Transmission Electron Microscopy: Bulk lipid cubic phase samples for cryogenic transmission electron microscopy (JEOL 2100 Cryo-TEM at 120 kV) were prepared on a lacey carbon-coated copper grid (Structure Probe Incorporation, PA) using a semi-automated Vitrobot (Vitrobot Mark II, FEI). Briefly, bulk lipid cubic phase samples were collected from flame sealed quartz capillaries by breaking them and 3 μL of 0.1 M samples was casted on top of a carbon grid. The grid was then transferred to a Vitrobot chamber at 100 % relative humidity and 4 ^{o}C. After blotting 3 times with 2 seconds blotting time, rapid immersion of the grid into liquid ethane effectively vitrifies the sample. Note that the samples should be kept under -170 ^{o}C until successfully transferred into the Cryo-TEM instrument in order to prevent crystalline ice formation. The images are obtained at a defocus of ~4000 nm.

POV-Ray Simulation: The diamond bicontinuous cubic phase (D) surface was generated using the level-set equations (Wohlgemuth et al., (2001) *Macromolecules* 34:6083–6089). By rotating the unit cell, we can generate a set of different images that can be used to match observed TEM data. Once we find the best match, thickness of the unit cell and number of unit cells are simulated to exactly match the observed magnification and shape. Images shown in Fig. 5 have a half of lattice parameter thickness.